INTERNATIONAL JOURNAL FOR NUMERICAL METHODS IN FLUIDS, VOL. 6, 541–556 (1986)

NUMERICAL SIMULATION OF SWIRLING FLOW IN DIFFUSERS

S. W. ARMFIELD AND C. A. J. FLETCHER

Department of Mechanical Engineering, University of Sydney, New South Wales 2006, Australia

SUMMARY

A reduced form of Navier–Stokes equations is developed which does not have the usual minimum axial step size restriction. The equations are able to predict accurately turbulent swirling flow in diffusers. An efficient single sweep implicit scheme is developed in conjunction with a variable grid size domain-conforming co-ordinate system. The present scheme indicates good agreement with experimental results for (1) turbulent pipe flow, (2) turbulent diffuser flow, (3) turbulent swirling diffuser flow. The strong coupling between the swirl and the axial velocity profiles outside of the boundary layer region is demonstrated.

KEY WORDS Turbulent Swirling Diffuser Flow Reduced Navier–Stokes Equations

1. INTRODUCTION

Diffuser augmented wind turbines offer an efficient means of generating electricity, both on the ground and in the jet stream.[1,2] The diffuser, when placed downstream of the turbine, converts dynamic pressure into static pressure and improves the efficiency. The flow through the diffuser is characterized by a significant positive pressure gradient and some swirl.

For maximum efficiency it is important that the diffuser does not stall, that is that the flow does not separate from the wall. There is evidence[3] that swirl can prevent the diffuser flow from separating at some diffuser angles, and thereby enable operation at larger diffuser area ratios with a correspondingly higher power output. Thus the ability to predict the flow behaviour is important in diffuser design.

It has been shown[4,5] that internal flows in ducts and pipes can be predicted using reduced forms of the Navier–Stokes equations, in which the axial diffusion terms are dropped. This reduction has the advantage of decreasing the computer time and storage required, compared to that required to solve the full Navier–Stokes equations.

The reduction is only possible when the flow is nearly 'parabolic', that is when the flow has minimal upstream influence. In this paper an order-of-magnitude analysis is used to show that a similar reduction is also valid for swirling flow in a diffuser, provided that both swirl and diffuser angle are small. The 'parabolic' requirement limits the prediction to non-reversing flows, as otherwise upstream behaviour is influenced significantly.

Conceptually similar reduced forms of the Navier–Stokes equations have been studied,[6,7] in relation to the flow around bodies in an otherwise undisturbed free stream. For external flows it is known[6] that the pressure can introduce an 'elliptic' behaviour, and this is responsible for imposing a minimum step size in the marching (axial) direction, to obtain a stable solution.

A similar pressure-induced instability can impose a minimum step size for internal flows.

0271–2091/86/080541–16$08.00

Received 13 May 1985
Revised 12 February 1986

However, Armfield and Fletcher[8] show that the order-of-magnitude neglect of terms in the radial momentum equation suppresses the destabilizing pressure behaviour, and with it the minimum axial step size restriction. This is particularly important in the present investigation, since a small axial step size is required to obtain locally accurate predictions.

A domain-conforming co-ordinate system is used, with cylindrical co-ordinates in the cylindrical section, and spherical co-ordinates in the diffuser section. This enables the equations to be solved in the simplest possible manner and allows the method to be easily adjusted to suit axisymmetric non-conical diffuser geometries.[9] Alternatively an orthogonal co-ordinate system may be generated using the Schwartz–Christoffel transformation and a potential flow solution.[10] However, this requires a computationally expensive iterative procedure to locate the unknown poles in the intermediate transform plane.

Since the flow is axisymmetric the equations are solved in the two-dimensional domain (x, r), where x is the axial co-ordinate and r the radial co-ordinate. The solution for the whole flow field is obtained by a single sweep in the x direction, using a sequence of one-dimensional calculations in the r direction.

The turbulent fluctuations are represented by Reynolds stress terms, which are modelled using an algebraic eddy viscosity closure. The Reynolds stresses can be reduced in a similar way to the other terms in the Navier–Stokes equations, so that the parabolic nature of the algorithm is unaffected.

The rest of the paper is arranged as follows. Section 2 provides details of the computational algorithm. First, the order-of-magnitude analysis and the method of solution are shown (sections 2.1–2.4). The turbulence model is described (section 2.5) and stability problems are outlined (section 2.6). Major alterations associated with the changeover from cylindrical to spherical co-ordinates are discussed (section 2.7). Comparison with experimental results is made in section 3, with emphasis on the relation between the swirl and axial velocity profiles in the diffuser.

2. COMPUTATIONAL ALGORITHM FOR INTERNAL SWIRLING FLOW

In this section it is shown that the Navier–Stokes equations may be reduced and that it is possible to solve them with a single sweep of the given domain in the flow direction. The main difficulty is that of determining the pressure field. Since internal flow is confined a mass flow constraint may be imposed, from which the axial pressure gradient is determined. However, the radial pressure gradient must be projected from the upstream solution.

An implicit scheme is derived, which is found to give improved stability and allow a coarser grid to be used, with accompanying savings in computing time, when compared with that required by an equivalent explicit scheme.

2.1. Formulation of the equations

The flow is considered to be axisymmetric, incompressible and of constant viscosity.

For cylindrical co-ordinates (x, r, ϕ), as shown in Figure 1, the velocity vector $\bar{\mathbf{V}}$ has components (u, v, w) in the axial, radial and circumferential directions, respectively. P is the pressure.

For $Re = \rho D U_m / v$, where D, the diameter of the cylinder, is the characteristic length and U_m, the mean axial velocity at the inlet, is the characteristic velocity, the non-dimensional governing equations for three-dimensional, steady, incompressible flow in (x, r, ϕ) co-ordinates are

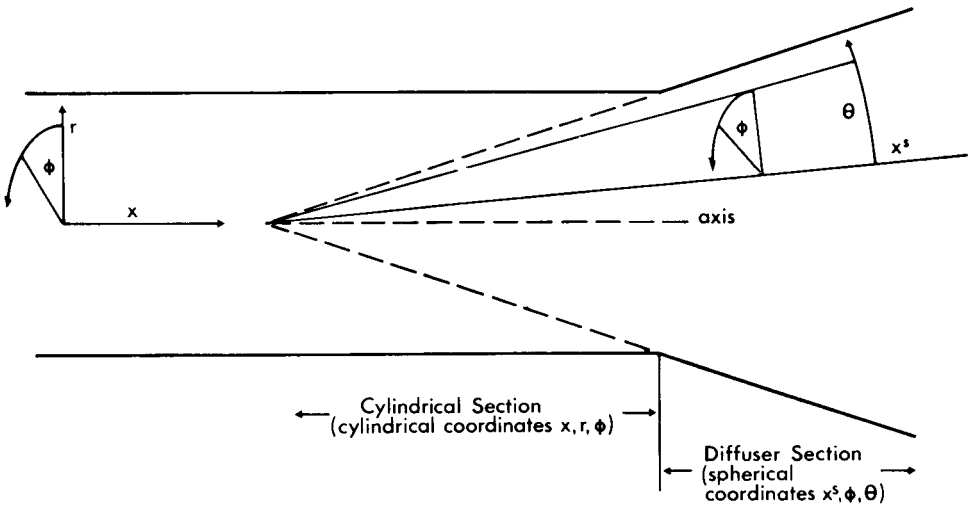

Figure 1. Co-ordinate systems

Momentum equations:

$$vu_r + uu_x = -P_x + \frac{1}{Re}[u_{rr} + u_r/r + u_{xx}], \tag{1}$$

$$vv_r + uv_x - w^2/r = -P_r + \frac{1}{Re}[v_{rr} + v_r/r + v_{xx} - v/r^2], \tag{2}$$

$$vw_r + uw_x + vw/r = \frac{1}{Re}[w_{rr} + w_r/r + w_{xx} - w/r^2]. \tag{3}$$

Continuity equation:

$$(rv)_r + ru_x = 0, \tag{4}$$

where subscripts denote partial differentiation.

To solve the system of equations (1)–(4) computationally, all variables must be stored at all nodal points, with multiple sweeps made over the domain. This requires large amounts of computer storage and time.

2.2. *Reduction of the governing equations*

It is shown, on an order-of-magnitude basis, that the Navier–Stokes equations may be reduced when the flow is nearly 'parabolic'. This is the case for non-separating pipe flow when the axial length is much greater than the diameter, i.e. away from the entry region. Also it is shown to hold for swirling diffuser flow, providing both the swirl and the diffuser angle are small. Once this reduction is made it is then possible to implement a single sweep marching algorithm.

The reduction of the governing equations is based on the following conditions:

(a) $L \gg R$
(b) $u \sim 1$

(c) $\delta \leqslant R$
(d) $w < u$

where L is pipe entry length, R is pipe radius, 0·5 in non-dimensional units and δ is boundary layer thickness.

Condition (a) will be valid everywhere except at the initial stages of developing pipe flow. Condition (b) comes from the non-dimensionalization. Condition (c) says the boundary layer cannot be greater than the cross-stream extent of the flow. Condition (d) is imposed to maintain positive axial velocity, and implies low swirl.

An order-of-magnitude analysis gives

$$\begin{aligned} u_x &\sim 1/L, \quad u_{xx} \sim 1/L^2, \quad u_r \sim 1/\delta, \quad u_{rr} \sim 1/\delta^2, \\ w_x &\sim W/L, \quad w_{xx} \sim W/L^2, \quad w_r \sim W/\delta, \quad w_{rr} \sim W/\delta^2, \\ v_x &\sim R/L^2, \quad v_{xx} \sim R/L^2, \quad v_r \sim 1/L, \quad v_{rr} \sim 1/RL, \end{aligned}$$

where W is the magnitude of the swirl.

Substitution into equations (1)–(4) shows that the $._{xx}$ terms can be dropped with little effect,[4] to give the reduced equations

$$uu_x + vu_r = -P_x + \frac{1}{Re}[u_{rr} + u_r/r], \tag{5}$$

$$uv_x + vv_r - w^2/r = -P_r + \frac{1}{Re}[v_{rr} + v_r/r - v/r^2], \tag{6}$$

$$vw_r + uw_x + vw/r = \frac{1}{Re}[w_{rr} + w_r/r - w/r^2], \tag{7}$$

$$(rv)_r + ru_x = 0. \tag{8}$$

The above set of equations is not parabolic, since terms in equation (6) introduce an elliptic-type behaviour, which has been demonstrated by showing that the characteristic polynomial has imaginary roots.[8] This behaviour introduces a severe stability reaction.[8] A similar destabilizing behaviour occurs in external flows.[6]

To remove this elliptic influence, equation (6) is further reduced by, first, splitting the pressure in the following manner:

$$P = P_1(x) + P_v(r, x) + P_w(r, x), \tag{9}$$

where $P_1(x)$ is the pressure at the axis, and $P_v(r, x)$, $P_w(r, x)$ are radially dependent components of P determined from equation (6) such that

$$(P_v)_r = -uv_x - vv_r + \frac{1}{Re}[v_{rr} + v_r - v/r^2],$$

$$(P_w)_r = w^2/r.$$

P_v can be interpreted as providing the radial variation of the pressure in non-swirling flows. Then P_w provides an additional radial variation due to swirl.

An order-of-magnitude analysis gives

$$\begin{aligned} P_v &\sim R/L^2, \\ P_w &\sim W^2; \end{aligned}$$

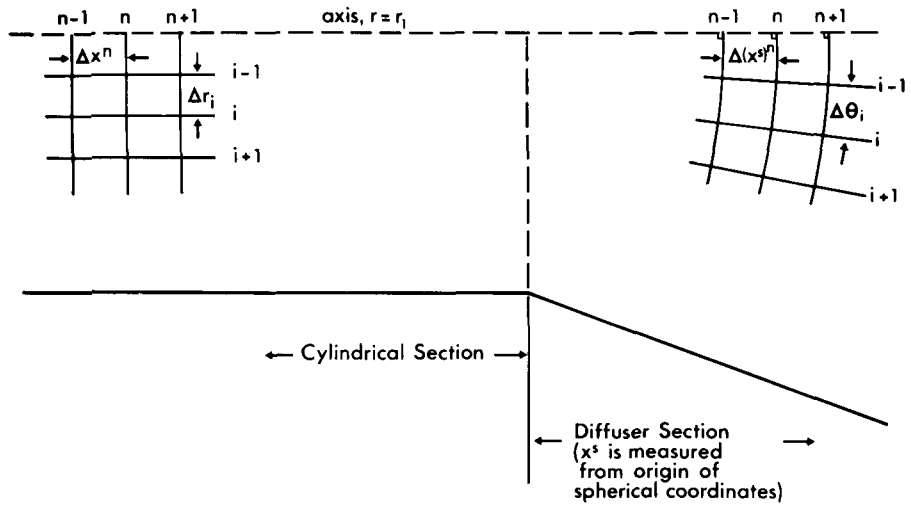

Figure 2. Grid notation

thus obtaining

$$P = P_1 + R/L^2 + P_w.$$

From equation (5) $P \sim 1$, and since $R/L^2 \ll 1$, P will now be defined as

$$P = P_1 + P_w,$$

rather than the definition given by equation (9). This enables equation (6) to be reduced to

$$P_r = w^2/r. \tag{10}$$

Equations (5), (10), (7) and (8) now provide the set of governing equations which will be solved numerically, together with the boundary conditions

$$\begin{aligned} u(R,x) = v(R,x) = w(R,x) = 0, \\ u_r(0,x) = v(0,x) = w(0,x) = 0, \\ 0 \leqslant x \leqslant X, \end{aligned} \tag{11}$$

where X is the total axial length and R is the radius at the wall.

2.3. *Discretization*

A rectangular mesh having variable Δx and Δr is used in the cylindrical section; in the diffuser section a radial mesh is used with variable Δx^s and $\Delta\theta$ (Figure 2).

In both regions the subscript i indicates location in the radial direction, with $i = 1$ indicating the axis and $i = k$ the wall. The superscript n indicates location in the axial direction.

The variables u, v and w are the exact solution of the initial boundary value problem, given by equations (5), (10), (7) and (8). These functions are approximated by discretizing equations (5), (10), (7) and (8) and solving the resulting system of algebraic equations to obtain the sets $\bar{u}(x^n, r_i)$, $\bar{v}(x^n, r_i)$, etc. When a solution is required away from nodal points it is obtained by linear interpolation.

The notation u_i^n will be used to denote a member of the set $\bar{u}(x^n, r_i)$; $u^n(r)$ will denote the exact solution to the ordinary differential equation obtained by discretizing in the x direction only. Variables v, w and P are treated in the same way.

2.4. *Method of solution*

The system of equations (5), (10), (7) and (8) is parabolic. Therefore it is solved numerically as an initial value problem in x. Discretizing in the x direction produces a system of non-linear ordinary differential equations. To linearize this system some terms are projected from upstream locations. This produces a linear system of equations in Δu_i^{n+1} and ΔP_i^{n+1} after discretizing in the r direction.

The linearization and projection introduce some first-order errors into what is otherwise a second-order scheme. For typical non-separating flows comparison with a fully second-order multi-sweep scheme has demonstrated that such an approximation leads to an error of no more than 1 per cent, and is justified on the grounds of computational efficiency. The discretized forms of equations (7), (10), (5) and (8) are solved at each station n to obtain w_i^{n+1}, $P_{w,i}^{n+1}$, u_i^{n+1} and v_i^{n+1}.

All terms are evaluated at station $n+\frac{1}{2}$, except u and v in equations (5) and (7). These terms are projected from upstream locations. This introduces a first-order approximation, and is potentially destabilizing, although, provided that the constraints (a), (b), (c) and (d) of section 2.2 are fulfilled, the influence is not great.

To obtain w_i^{n+1} equation (7) is discretized in the x direction to give,

$$u^n \Delta w^{n+1}/\Delta x^{n+1} = G(w^{n+1/2}, v^{n+1/2}, r) + O(\Delta x^2),$$

where

$$G(w^{n+1/2}, u^{n+1/2}, v^{n+1/2}, r) = \frac{1}{Re}[w_{rr}^{n+1/2} + w_r^{n+1/2}/r - w^{n+1/2}/r^2] - v^{n+1/2} w_r^{n+1/2} - \frac{v^{n+1/2} w^{n+1/2}}{r}.$$

The linear differential operator G is discretized using

$$[w(x^n, r_i)]_r = \frac{(w_{i+1}^n - w_{i-1}^n)}{(\Delta r_{i+1} + \Delta r_i)} + O(\Delta r^2),$$

$$[w(x^n, r_i)]_{rr} = \left(\frac{(w_{i+1}^n - w_i^n)}{\Delta r_{i+1}} - \frac{(w_i^n - w_{i-1}^n)}{\Delta r_i}\right) \Big/ \frac{(\Delta r_{i+1} + \Delta r_i)}{2} + O(\Delta r^2),$$

where

$$\Delta r_{i+1} = r_{i+1} - r_i,$$

to obtain $\bar{G}(w_i^n, u_i^{n+1/2}, v_i^{n+1/2} r_i)$, the discretized version of G, giving the following linear system in Δw_i^{n+1}:

$$[(u_i^{n+1/2}/\Delta x^{n+1/2})I - \bar{G}(u_i^{n+1/2}, v_i^{n+1/2}, r_i)/2]\Delta w_i^{n+1} = \bar{G}(w_i^n, u_i^{n+1/2}, v_i^{n+1/2}, r_i) + O(\Delta x^2, \Delta r^2), \quad (12)$$

The terms w_i^{n+1} are obtained by solving the tridiagonal system resulting from equation (12).

To obtain $P_{w_i}^{n+1}$, equation (10) is discretized to produce

$$P_{w_{i+1}}^{n+1} = \Delta r_{i+1}\left(\frac{(w_{i+1}^{n+1} + w_i^{n+1})^2}{2}\right) \Big/ r_{i+1/2} + P_{w_i}^{n+1} + O(\Delta r^2),$$

with $P_{w_1}^{n+1} = 0$.

Thus the radial variation of P is entirely dependent on the swirl, and is obtained using a second-order scheme.

To obtain u_i^{n+1} the following procedure is used. First equation (5) is discretized in the x direction to obtain

$$u^n \frac{(\Delta u^{n+1})}{\Delta x^{n+1}} = J(u^{n+1/2}, v^{n+1/2}, r) - \frac{\Delta P^{n+1}}{\Delta x^{n+1}} + O(\Delta x), \tag{13}$$

where

$$J(u^{n+1/2}, v^{n+1/2}, r) = \frac{1}{Re}\left[u_{rr}^{n+1/2} + \frac{u_r^{n+1/2}}{r} \right] - v^{n+1/2} u_r^{n+1/2},$$

and

$$\Delta u^{n+1} = u^{n+1} - u^n,$$

$$\Delta P^{n+1} = P^{n+1} - P^n,$$

$$u^{n+1/2} = 0{\cdot}5(u^n + u^{n+1}),$$

$$v^{n+1/2} = \tfrac{3}{2} v^n - \frac{v^{n-1}}{2},$$

$$\Delta x^{n+1} = x^{n+1} - x^n.$$

Subsequent manipulation produces the following linear system in Δu^{n+1}:

$$\left[u^n \frac{\Delta u^{n+1}}{\Delta x^{n+1}} - J\left(\frac{\Delta u^{n+1}}{2}, v^{n+1/2}, r \right) + \frac{\Delta P^{n+1}}{\Delta x^{n+1}} \right] = J(u^n, u^{n+1/2}, r). \tag{14}$$

Discretizing J in the r direction to obtain $\bar{J}$ then gives,

$$|(u_i^n/\Delta x^{n+1})I - \bar{J}(v_i^{n+1/2}, r_i)/2|\Delta u_i^{n+1} + \Delta P_i^{n+1}/\Delta x^{n+1} = \bar{J}(u_i^n, v_i^{n+1/2}, r_i) + O(\Delta x, \Delta r^2). \tag{15}$$

This produces a system of linear algebraic equations in the unknowns Δu_i^{n+1} and ΔP_i^{n+1}, with coefficients $C_{i,j}$, of the form

$$\begin{aligned} C_{2,1}\,\Delta P_2^{n+1} + C_{2,2}\,\Delta u_1^{n+1} + C_{2,3}\,\Delta u_2^{n+1} + C_{2,4}\,\Delta u_3^{n+1} &= C_{2,5}, \\ &\vdots \\ C_{k-1,1}\,\Delta P_{k-1}^{n+1} + C_{k-1,2}\,\Delta u_{k-2}^{n+1} + C_{k-1,3}\,\Delta u_{k-1}^{n+1} + C_{k-1,4}\,\Delta u_k^{n+1} &= C_{k-1,5}. \end{aligned} \tag{16}$$

Since equation (15) is singular at $r = 0$, $C_{1,j}$ cannot be calculated as the other $C_{i,j}$ are. As the system (16) requires one more equation containing the $C_{1,j}$ to make it invertible, this is obtained by writing Δu_1^{n+1} in terms of Δu_2^{n+1} and Δu_3^{n+1} by passing a quadratic through Δu_2^{n+1} and Δu_3^{n+1}. Alternatively, L'Hospitals rule may be used, but as this reduced the stability without leading to greater accuracy for the flows considered, the above approach was followed.[9]

The pressure term, ΔP_i^{n+1}, is handled as follows: from section 2.2

$$\Delta P_i^{n+1} = \Delta P_1^{n+1} + \Delta P_{w,i}^{n+1}.$$

ΔP_1^{n+1} is ΔP at the axis, $\Delta P_{w,1}^{n+1}$ is obtained as $P_{w,i}^{n+1} - P_{w,i}^n$.

With the pressure split in this manner the system (16) may be inverted to obtain

$$\Delta u_i^{n+1} = f_i^{n+1} + g_i^{n+1}\,\Delta P_1^{n+1}. \tag{17}$$

ΔP_1^{n+1} is unknown and is obtained following Briley,[5] by[9] integrating equation (8) w.r.t. radius and substituting for Δu in terms of f, g and ΔP as given in equation (17). Manipulation gives

$$\Delta P_1^{n+1} = \frac{\int_0^R -rf^{n+1}\,\mathrm{d}r}{\int_0^R rg^{n+1}\,\mathrm{d}r}, \tag{18}$$

since ${}_{0\phi} = 0$.

To obtain v_i^{n+1} equation (8) is discretized to give

$$v_{i+1/2}^{n+1/2} + r_{i+1/2}(v_{i+1}^{n+1/2} - v_i^{n+1/2})/\Delta r_{i+1} = -r_{i+1/2}\,\Delta u_{i+1/2}^{n+1}/\Delta x^{n+1}, \tag{19}$$

where $v_{i+1/2}^{n+1/2} = (v_i^{n+1/2} + v_{i+1}^{n+1/2})/2$, and similarly for other variables. Therefore,

$$v_{i+1}^{n+1/2} = \frac{(-r_{i+1/2}(\Delta u_{i+1/2}^{n+1}/\Delta x^{n+1}) - v_i^{n+1/2}(\frac{1}{2} - r_{i+1/2}/\Delta r_{i+1}))}{(\frac{1}{2} + r_{i+1/2}/\Delta r_{i+1})}, \tag{20}$$

with $v_1^{n+1/2} = 0$ and $v_{i+1}^{n+1} = 2v_{i+1}^{n+1/2} - v_{i+1}^n$.

The equivalent explicit forms of equations (12) and (14) are

$$\Delta w^{n+1} = \bar{G}(w^n, u^n, v^n, r)\frac{\Delta x^{n+1}}{u^n}, \tag{12'}$$

$$\Delta u^{n+1} = (-\Delta P^{n+1}/\Delta x + \bar{J}(u^n, v^n, r))/\frac{\Delta x^{n+1}}{u^n}. \tag{14'}$$

2.5. *Reynolds stress closure*

To obtain the solution when the flow is turbulent, Reynolds stresses are added to the right hand side of the momentum equations as

equation (5): $-(\overline{u'v'})_r - \dfrac{\overline{u'v'}}{r} - (\overline{u'u'})$,

equation (6): $-(\overline{v'v'})_r - \dfrac{(\overline{v'v'})}{r} - (\overline{v'u'})_x + \dfrac{\overline{w'w}}{r}$,

equation (7): $-(\overline{v'w'})_r - (\overline{u'w'})_x - 2\dfrac{(\overline{v'w'})}{r}$.

An order-of-magnitude argument, after Koonsinlin and Lockwood,[12] allows these expressions to be approximated as,

equation (5): $-(\overline{u'v'})_r - \dfrac{(\overline{u'v'})}{r}$,

equation (6): 0,

equation (7): $-(\overline{v'w'})_r - 2\dfrac{(\overline{v'w'})}{r}$.

To relate the approximate Reynolds stresses to the mean flow the following eddy viscosity model is used:[13]

$$(\overline{u'v'}) = \nu_x \frac{\partial u}{\partial y},$$

$$(\overline{w'v'}) = \nu_\phi \left(\frac{\partial w}{\partial y} + \frac{w}{r} \right),$$

where ν_x is the eddy viscosity related to the axial velocity, and ν_ϕ is the eddy viscosity related to the swirl, and $y = R - r$.

ν_x and ν_ϕ are then obtained in the low shear region near the axis as

$$\nu_x = \nu_\phi = 0{\cdot}0168\,\delta^* u_a, \tag{21}$$

where

$$\delta^* = \int_0^R 2r(1 - q_t)\,dr$$

and

$$q_t^2 = (u^2 + w^2)/u_a^2,$$

with $u_a = u$ at the axis.

In the high shear region close to the wall ν_x and ν_ϕ are obtained as

$$\nu_x = \frac{r}{R} l_x^2 \left[(u_r)^2 + \left(\frac{1}{\sigma} \right) \left(r \left(\frac{w}{r} \right)_r \right)^2 \right]^{1/2}, \tag{22}$$

where

$$\sigma = \frac{\nu_x}{\nu_\phi} \tag{23}$$

and

$$l_x = KR \ln\left(\frac{R}{r} \right) \left\{ 1 - \exp\left[-R \ln\left(\frac{R}{r} \right) Re\, \tau_{xw}^{1/2} / A \right] \right\}, \tag{24}$$

$$\nu_\phi = \frac{r}{R} l_\phi^2 \left\{ (u_r)^2 + \frac{1}{\sigma} \left[r \left(\frac{w}{r} \right)_r \right]^2 \right\}^{1/2}, \tag{25}$$

where

$$l_\phi = KR \ln\left(\frac{R}{r} \right) \left\{ 1 - \exp\left[-R \ln\left(\frac{R}{r} \right) Re\, \tau_{\phi w}^{1/2} / A \right] \right\}, \tag{26}$$

the von Karman constant, $K = 0{\cdot}41$, and A is a pressure gradient correction term of the form

$$A = \frac{26}{\{1 - 11{\cdot}8[u_a(u_a)_x]\}^{1/2}}.$$

The Reynolds stress terms are included in the implicit formulation by projecting ν_x and ν_ϕ from upstream locations, which allows the terms $\nu_x \partial u/\partial r$ and $\nu_\phi \partial w/\partial r$ to be formulated in the same way as other r derivatives. Not treating the Reynolds stresses implicitly was found to produce an axial step-size restriction.

As can be seen the only difference between v_ϕ and v_x arises from the l_x and l_ϕ terms. The change-over from equations (22) and (25) to equation (21) is made when v_x in the near wall region equals v_x in the near axis region, and v_ϕ in the near wall region equals v_ϕ in the near axis region.

2.6. *Stability of the scheme*

A problem with single sweep marching is the amplification of any error which cannot be controlled by a relaxation factor, as it can often be in multi-sweep techniques. This can lead to severe stability and accuracy problems.

As has been mentioned previously, this instability is associated with the 'elliptic' pressure interaction.[6,8] Instability can also arise as a result of round-off error, or the error introduced by linearization. The use of an implicit scheme is necessary to damp the potentially unstable behaviour, which is particularly significant in turbulent swirling diffuser flow. The implicit scheme is more accurate than an equivalent explicit scheme, allowing a larger axial step size to be used.[8]

2.7. *Diffuser section*

In the diffuser section the governing equations are written in terms of spherical co-ordinates x^s, ϕ, θ, as shown in Figure 1. The spherical radius is denoted by x^s rather than r^s to avoid confusion with the cylindrical radius, and to maintain the convention of using the symbol x as the axial (marching) ordinate.

For a velocity vector $\bar{\mathbf{U}}$, the components in the axial, radial and circumferential directions are (u^s, v^s, w^s), respectively.

The relation between (u^s, v^s, w^s) and (u, v, w) at the diffuser entrance is

$$\begin{aligned} u^s &= u\cos\theta + v\sin\theta, \\ v^s &= v\cos\theta - u\sin\theta, \\ w^s &= w, \end{aligned} \tag{27}$$

where θ is the local angle between u^s and u.

The reduction of the equations is similar to that for flow in the cylindrical section (Figure 2) except for an additional limitation on the diffuser angle arising from constraint (c) of section 2.2. That is, to maintain the condition $v^s \ll u^s$, the diffuser total angle must be less than 13°.[9]

The resulting set of reduced equations may be solved as in the cylindrical section (Figure 2), with x^s, the radius of the sphere, being the direction of marching. A discretization and algebraic manipulation equivalent to that described in sections 2.3 and 2.4 are carried out.[9] The resulting equations, equivalent to equations (12), (15), (18) and (20) provide corrections to the solution, Δu^{n+1}, etc., in the diffuser. The main change is that in the diffuser the axial velocity must decrease to maintain a constant mass flow. This results in a different mass flow integral,[9] which is obtained simply by integrating the equation of continuity in spherical co-ordinates.

3. RESULTS AND DISCUSSION

3.1. *Pipe flow*

For non-swirling flow the algorithm is tested against the results of Barbin and Jones[14] for developing turbulent flow in a constant diameter pipe. The starting profile for the computation matches the entrance flow to the pipe, at a Reynolds number of 388,000 (based on diameter).

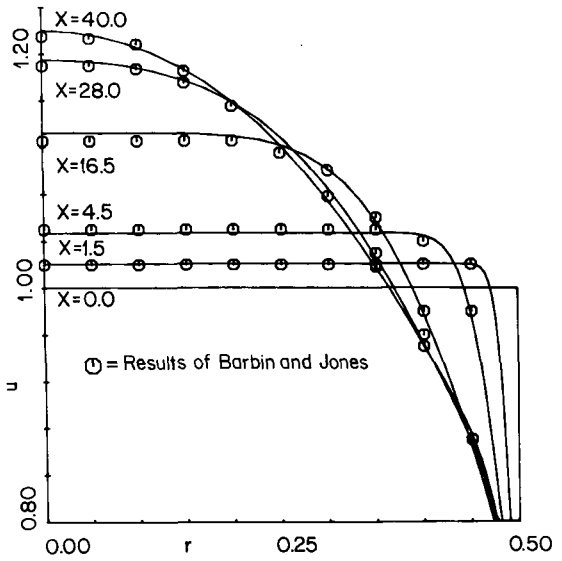

Figure 3. Developing velocity profiles for turbulent pipe flow

The development of the axial velocity distribution is shown in Figure 3. As can be seen, good agreement is obtained both for developing and fully developed flow.

To obtain an accurate and mesh independent solution a minimum radial step of 0·001 of a diameter is used at the wall. The radial grid increases by 10 per cent in moving away from the wall, with a maximum of 0·03 of a diameter at the axis. This leads to fifty points in the radial direction, with nineteen points in the 10 per cent of the domain nearest the wall. A starting axial step size of 0·01 of a diameter was found to give accurate mesh independent results, with a gradual increase as the flow approached full development, resulting in a step-size of 0·05 at $x = 40$ diameters.

Strictly the condition $R \ll L$, on which the present method is based, is not vaid right at the entrance to the pipe. Clearly, from Figure 3, any error that violating this condition causes has a negligible influence on the downstream development of the solution.

The predicted eddy viscosity is compared with the experimental results of Richman and Azad[15] for fully developed turbulent pipe flow. Figure 4 shows the variation of the eddy-viscosity, times by the Reynolds number, with radius. As can be seen, within the limitations of the model, the computed eddy-viscosity is behaving in the same fashion as the experimental data.

No attempt, using an intermittency factor, has been made to match the fall-off in eddy-viscosity close to the axis, as this has little effect on the fully developed velocity profile for turbulent pipe flow, which is predicted accurately (Figure 3).

3.2. *Diffuser flow*

To test the algorithm for non-swirling diffuser flow the results of Fraser[16] are used. In this case the entry flow is that of a boundary layer plus inviscid core at a length Reynolds number of 386,000. The flow develops in a conical diffuser of total angle 10°, which produces a severe adverse pressure gradient.

Figure 5 shows the axial velocity at the diffuser entrance and at a point approximately 1·4 diameters downstream, compared with the experimental velocity profiles of Fraser. As can be seen the reduction in the average velocity and the change in the velocity profile are predicted accurately.

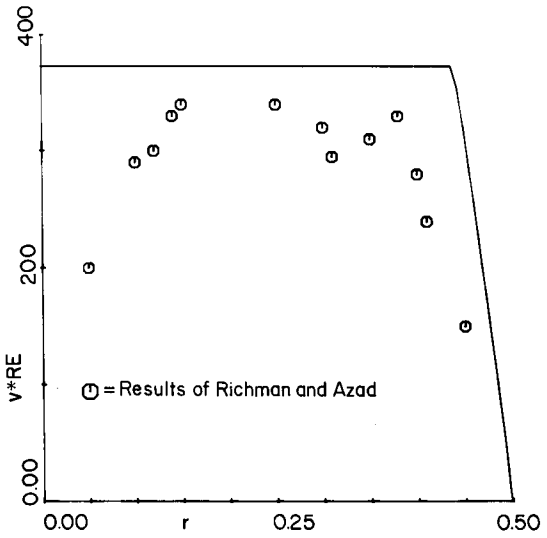

Figure 4. Radial variation of eddy viscosity for fully developed pipe flow

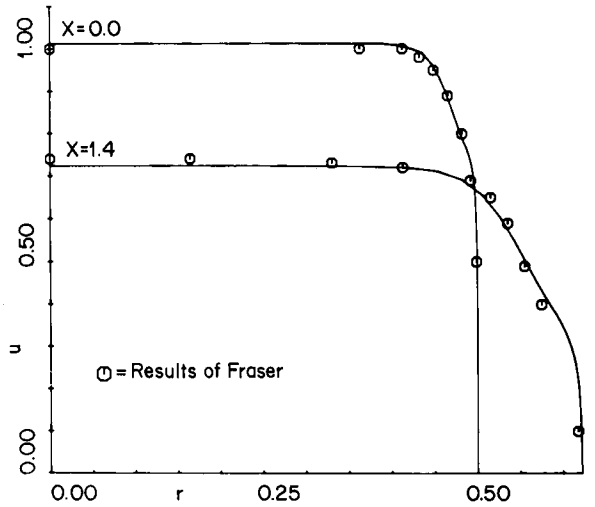

Figure 5. Velocity profiles for non-swirling flow in a conical diffuser

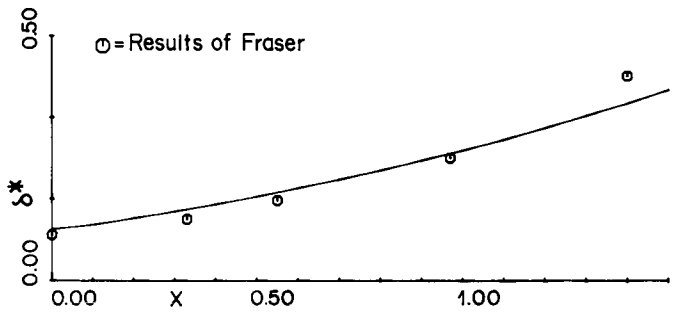

Figure 6. Axial variation of displacement area in a conical diffuser

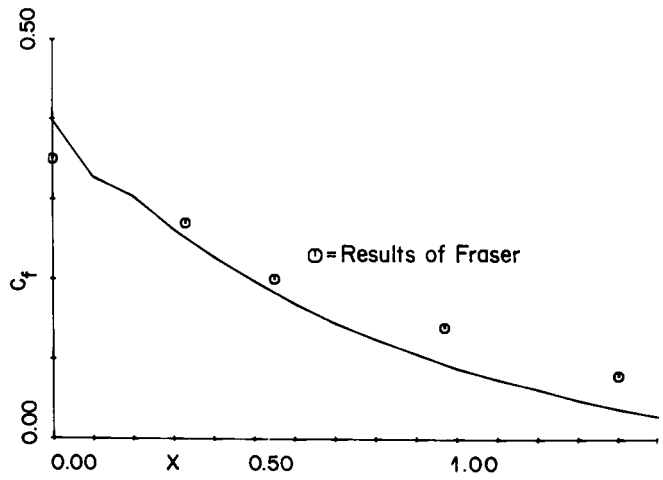

Figure 7. Axial variation of skin friction in a conical diffuser

The increase in displacement area with downstream location is shown in Figure 6 and corresponds closely to that obtained experimentally by Fraser. The displacement area is defined as δ^* in equation (21). Figure 7 shows the axial skin friction component obtained from

$$C_f = \frac{2}{Re}\frac{\partial u}{\partial y}\bigg|_w.$$

As can be seen, the magnitude of axial skin friction drops rapidly in the diffuser, and is in good agreement with Fraser's results except for a slight underprediction at downstream locations.

The skin friction is proportional to the normal velocity gradient at the wall and is a very sensitive parameter to predict accurately. In addition the flow in a 10° conical diffuser is close to separation and the assumptions inherent in the present reduced formulation are less valid under these conditions.

For the diffuser flow it is found that a mesh similar to that used in the constant diameter pipe gives accurate mesh independent results. That is a radial step of 0·001 of a diameter at the wall with a graduated increase of 10 per cent, and a starting axial step of 0·01 of a diameter.

The results of So[17] are used to test the algorithm for swirling flow in a diffuser. So presents a series of results for flow in a 7° conical diffuser at a Reynolds number, based on entrance diameter, of 382,000, with varying degrees of swirl. Comparison is made with the case of no swirl, Figures 8 and 9, with swirl with a w_{av}/u_{av} number of 0·3, Figures 10–12.

To produce the flow So used an apparatus with a centrifugal blower, and no cylindrical section before the diffuser entrance to enable readings to be taken. Thus the first velocity profile given is actually half a diameter inside the diffuser.

To match this first profile various starting profiles were tried at the diffuser entrance with the best match being used. As can be seen from Figure 8 even for the case of no swirl the first profile has a dip at the axis. This presumably is due to the blowing arrangement previously mentioned.

Despite these difficulties the reduction in average velocity, and the downstream development predicted for both axial velocity (Figure 8) and pressure (Figure 9) agree well with So's results. It can be seen from the pressure obtained experimentally by So that, in non-swirling flow, the radial variation in pressure is close to zero, as was assumed in section 2.2.

The most notable effect of the inclusion of swirl on the axial velocity (Figure 10) is the marked dip in axial velocity at the axis.

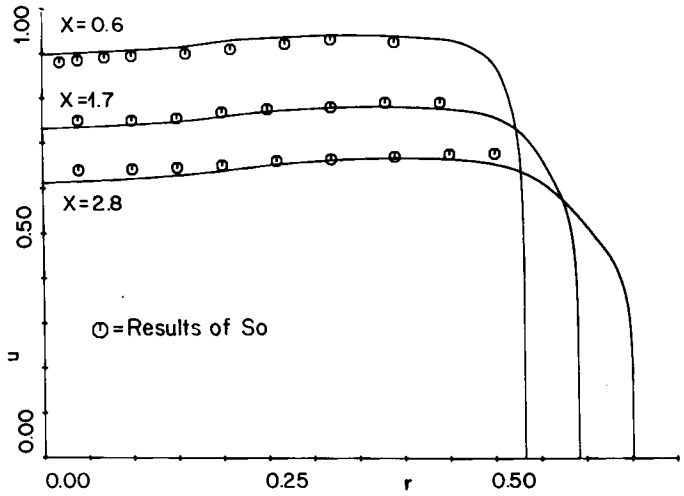

Figure 8. Comparison with non-swirling velocity profiles of So

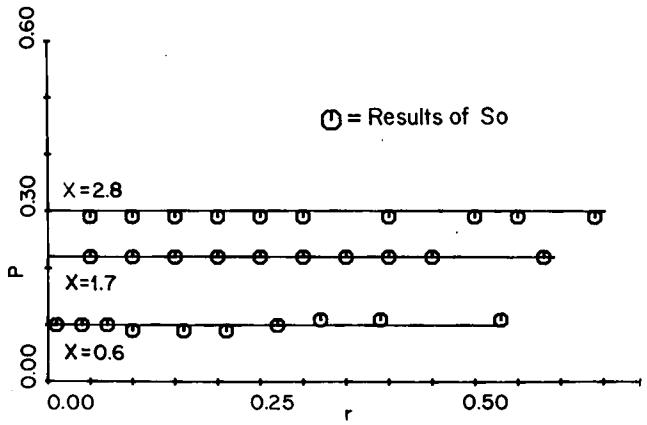

Figure 9. Pressure distribution in non-swirling diffuser-flow

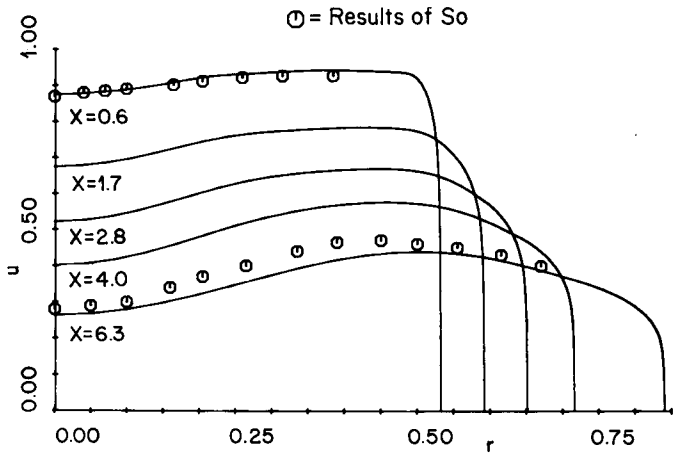

Figure 10. Axial velocity variation for swirling diffuser flow

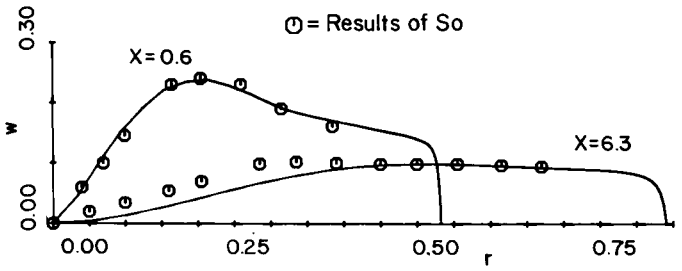

Figure 11. Circumferential velocity variation for swirling diffuser flow

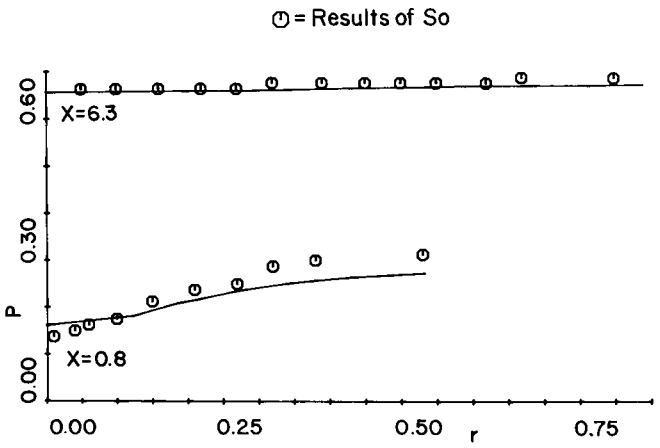

Figure 12. Pressure distribution for swirling diffuser flow

Figure 11 shows the circumferential velocity profile. As can be seen the algorithm models the decay of swirl well. This is particularly important as it is the decay of swirl that leads to the reduction in axial velocity at the axis.

The effect of swirl of producing a positive radial pressure gradient is apparent in Figure 12; clearly the algorithm models this effect.

3.3. Discussion

The reduced Navier–Stokes equations are used to model flows where the constraints of section 2.2 are satisfied. To enable a single sweep algorithm to be used it is important to be able to show that the non-swirling radial component of pressure is small enough to be discarded, once the pressure is split as in equation (10). That this is the case for diffuser flow is clear from Figure (9), where the pressure is shown experimentally to be very close to constant across the radius.

For flow with swirl the main contribution to the radial pressure gradient comes from the swirl itself, as is clear from comparing Figures 9 and 12.

The reduction in axial velocity at the axis resulting from the inclusion of swirl can be seen in Figure 10. The accompanying relative increase in axial velocity near the wall will aid in the prevention of separation at a given area ratio.

An implicit formulation of Crank–Nicolson type has been developed. This was done to enable a larger axial step size to be used, while still retaining the required accuracy. The implicit formulation is computationally more expensive, requiring about 20 per cent more time per step, than an

equivalent explicit scheme. For turbulent pipe flow it was found that to maintain stability a maximum Δx of 0·005 was required, using the explicit scheme. For the implicit scheme a starting axial step-size of 0·01 was used. However with an axial step-size of 0·02 the solution changed by only 1 per cent in the axial velocity component.

4. CONCLUSIONS

The order-of-magnitude exclusion of the P_v component from the radial momentum equation and the axial viscous diffusion terms from all the momentum equations is shown to produce an efficient single sweep algorithm for turbulent swirling flow in diffusers.

The single sweep algorithm is able accurately to predict, based on the agreement with experimental data, turbulent pipe flow and both swirling and non-swirling flows in conical diffusers.

The reduced Navier–Stokes equations clearly demonstrate the strong coupling between swirl and the axial velocity profile outside of the boundary layer region, and demonstrate the manner in which swirl aids in the prevention of separation at a given diffuser angle.

ACKNOWLEDGEMENT

The authors are grateful to the Australian Research Grants Committee for their continuing support of the research on internal swirling flows.

REFERENCES

1. C. A. J. Fletcher, A. J. Honan and J. S. Sapuppo, 'Aerodynamic platform comparison for jet-stream electricity generation'. *J. Energy*, **7**, 17–23 (1983).
2. C. A. J. Fletcher and B. W. Roberts, 'Electricity generation from jet-stream winds', *J. Energy*, **3**, 241–249 (1979).
3. Y. Senoo, N. Kawaguchi and T. Nagata, 'Swirl flow in conical diffusers', *Bull. J.S.M.E.*, **21**, 112–119 (1978).
4. D. Yaschin, M. Israeli and M. Wolfshtein, 'Numerical solutions of the parabolized three-dimensional steady flow in axially symmetric pipes', in J. Noye and C. Fletcher (eds), *Computational Techniques and Applications CTAC-83*, North-Holland, 1984, pp. 533–552.
5. W. Briley, 'Numerical method for predicting three-dimensional steady flow in ducts', *J. Comp. Phys.*, **14**, 8–28 (1974).
6. S. G. Rubin, 'A review of marching procedures for parabolized Navier–Stokes equations', in T. Cebeci (ed), *Proc. 1st Symposium on Num. Aspects of Aero. Flows*, Springer-Verlag, 1981, pp. 171–186.
7. S. G. Rubin, 'Global relaxation procedures for a reduced form of the Navier–Stokes equations', *Proc. Ninth Int. Conf. Num. Methods in Fluid Dynamics*, Paris, 1984, *Lecture Notes in Physics, 218*, Springer-Verlag, Heidelberg, 1985, pp. 62–71.
8. S. W. Armfield and C. A. J. Fletcher, 'Pressure related instabilities of reduced Navier–Stokes equations for internal flows', *Commun. appl. numer. methods*, **2**, 377–383 (1986).
9. S. W. Armfield, 'Internal swirling flow', *Ph.D. Thesis*, University of Sydney, Australia, 1985.
10. O. L. Anderson, 'Calculation of internal viscous flows in axisymmetric ducts at moderate to high Reynolds numbers', *Computers and Fluids*, **8**, 391–411 (1980).
11. T.Cebeci and A. M. O. Smith, *Analysis of Turbulent Boundary layers*, Academic Press, New York, 1974, pp. 64–71.
12. M. L. Koonsinlin and F. C. Lockwood, 'The prediction of axisymmetric swirling boundary layers', *A.I.A.A. Journal*, **12**, (4), 547–554 (1974).
13. C. A. J. Fletcher, 'Application of the Dorodnitsyn finite element method to swirling boundary layer flow', *Int. j. numer. methods in fluids*, **5**, 443–462 (1985).
14. A. R. Barbin and J. B. Jones, 'Turbulent flow in the inlet region of a smooth pipe', *J. Basic Eng. A.S.M.E.*, **85**, 29–34 (1963).
15. J. W. Richman and R. S. Azad, 'Developing turbulent flow in smooth pipes', *Appl. Sci. Res.*, **28**, 419–441 (1973).
16. H. R. Fraser, 'Study of an incompressible turbulent boundary layer in a conical diffuser', *Ph.D. Thesis*, University of Illinois (1956); see also *Proc. A.S.C.E. (J. Hydr. Div.)*, **84**, 1684/1–17 (1958).
17. K. L. So, 'Vortex decay in a conical diffuser', *Report No. 75*, Gas Turbine Lab, M.I.T., September 1964.